J Mater Sci: Mater Electron (2017) 28:9658–9666
DOI 10.1007/s10854-017-6716-x

A novel all-organic DIPAB/PVDF composite film with high dielectric permittivity

Wenlong Yang[1] · Haidong Li[1] · Jiaqi Lin[1,2] · Gaoru Chen[2] · Yu Wang[1] · Li Wang[1] · Haowei Lu[1] · Liangyu Chen[3] · Qingquan Lei[2]

Received: 5 November 2016 / Accepted: 7 March 2017 / Published online: 14 March 2017

Abstract A novel all-organic composite comprising polyvinylidene fluoride (PVDF) and diisopropylammonium bromide (DIPAB) crystal particles (0–20 mass%) with significant dielectric properties has been synthesized via coating method. The DIPAB crystal nano-particles were prepared in the PVDF matrix by in situ growth method, which were found effective in transforming structure and enhancing the dielectric properties of the composites. X-ray diffraction pattern and Fourier transform infrared spectroscopy confirmed that the DIPAB in situ particles can improve the content of the electroactive β phase nucleation in PVDF matrix, whereas the PVDF matrix could induce the (00*l*) preferred orientation of the DIPAB nano-crystal. And the dielectric performance of the DIPAB/PVDF composite was significant influenced by the enhanced electroactive β phase and (00l) textured DIPAB. Relative dielectric constants as high as 94 was obtained at 40 Hz with 5 mass% DIPAB filler, which is 11-fold higher than that of the pure PVDF matrix (~8.5). The breakdown strength decreased as the mass fraction of DIPAB increased but still stayed more than 38.9 kV/mm.

✉ Wenlong Yang
yangwenlong1983@163.com

[1] Department of Applied Science, Harbin University of Science and Technology, Harbin 150080, People's Republic of China

[2] Key Laboratory of Engineering Dielectrics and Its Application, Ministry of Education, Harbin University of Science and Technology, Harbin 150080, People's Republic of China

[3] School of Mathematics and Science, Jiangsu University of Science and Technology, Zhenjiang 212003, Jiangsu, People's Republic of China

1 Introduction

High energy density materials have attracted increasing attention because of their potential application in advanced electronic devices and electric power systems [1–3]. The stored energy density, U, is equal to $U=\int EdD$, where E is the applied electric field, and D is the electric displacement [4]. For linear dielectrics, the equation could be approximated as $U=1/2\varepsilon_0\varepsilon_r E_b^2$, where ε_0, ε_r and E_b are the vacuum dielectric permittivity, the relative permittivity and the breakdown electric field, respectively. Therefore, both high dielectric permittivity, ε_r, and the breakdown electric field, E_b, are essential issues for the high energy density materials [5].

Many flexible polymers such as polyvinylidene fluoride (PVDF) [6], polyimide (PI) [7] and polyethylene (PE) [8], have especially high breakdown electric field ($E_b \geq 100$ kV/mm under low frequency) and excellent processing properties. However, the low dielectric permittivity ($\varepsilon_r \leq 10$) restrains their applications in energy density storage [9]. Therefore, one of the key issues is improving the dielectric permittivity of the polymer materials. It is well known that the Clussius Equation, $P=\varepsilon_0(\varepsilon_r-1)E=N\alpha E_i$, could be used to design the dielectric permittivity of the material, where P, E, N, α and E_i are the intensity of dielectric polarization, the macroscopic electric field intensity, the molecule number in unit volume, polarizability and the effective electric field intensity on molecular in the materials, respectively. This equation represents the relationship between the macroscopic parameters of material and its microscopic parameters. The relative dielectric constant of the material will increase when the internal polarization rate per unit volume increases.

In order to obtain high dielectric constant composites, researchers have developed many types of inorganic and

organic fillers. On the one hand, the ferroelectric and/or piezoelectric ceramic particles with higher polarizability such as barium titanate (BT) [10], lead–zirconium–titanate (PZT) [11], barium-calcium-zirconium-titanate (BCZT) [12] and alkaline niobate (KTN) [13] are effective fillers. Indeed, the relative dielectric constant of PVDF can be improved from 9.3 to 44.3 by doping of 30 vol% $BaTiO_3$ nanowires with an aspect ratio of 45.8 [14]. The relative dielectric constant of PZT/PVDF composites could be 80 with 30 vol% loading [15]; and the composites with high doping concentration of BCZT and KTN particles exhibit dielectric constant 50–80 [16, 17]. However, there are some difficulties with high doping concentrations: (i) The dispersivity of nano-particles in the polymer matrix is hard to control, especially with high loading concentrations. Because of the high surface energy of the nano-particles—particles are likely to agglomerate in the matrix. (ii) The mechanical properties of the composites decrease rapidly with increasing doping concentration of inorganic fillers. Most of composite films are fragile when the doping concentration is more than 30 vol%. Weak Van der Waals forces are the dominant interaction between the matrix and the unmodified particles; the large amount of inorganic particles reduces the inter-molecular forces of the polymer. (iii) The breakdown electric fields of the composites will obviously decrease versus pure polymers. This is because the increasing defects will intensify the distortion of electric field; and the partial breakdown likely occurs inside the material. Therefore, the breakdown electric field of ceramic/PVDF composite flexible films decreases sharply [16].

The dielectric composites with conductive fillers such as silver (Ag), nickel (Ni) and carbon nanotubes also exhibit high dielectric permittivity. The composites possess lower dielectric loss and independent frequency performance under lower doping concentration because of the rapid response of the electron displacement polarization in the conductive particles. However, the conductivity of composite will rapidly increase and the dielectric loss becomes larger when the filling concentration approaches the percolation threshold. It is important to note that the percolation thresholds of the composites (silver/polyimide ~0.122 [18], Ni/PVDF ~0.17 [19] and carbon nano-tubes/PVDF ~0.0161 [20]) are lower, which restrains the adjustable range of dielectric constant.

All organic composite materials with a high dielectric constant have received increasing attention due to their low density and flexibility [21]. They can possess excellent mechanical and processing properties even with higher concentrations of organic fillers—this differs from the inorganic fillers' composites because of the high consistency and strong interactions between the fillers and the matrix. The all organic dielectric composites also have lager adjustable range because of their higher consistency [22, 23].

Here, an advanced all organic composite film with high dielectric permittivity that contains diisopropylammonium bromide (DIPAB) as a functional filler and thermoplastic PVDF with superior performance as the polymer matrix was designed. The DIPAB was selected as the organic filler due to its high spontaneous polarization (23 $\mu C/cm^2$) [24], easy processing and good compatibility with polymer matrix—this gives an advantage in the dispersion of DIPAB even at high loading concentration, which reduces the loss tangent and maintains high E_b in the matrix. The PVDF is a popular material with excellent mechanical and electrical performance and relatively high dielectric constant at room temperature (8–12 at 10^2 Hz). This makes it suitable for advanced electronic devices and electric power systems [4, 9].

Due to the unique growth characteristics of DIPAB crystal, it is suitable for in situ nucleation and growth in PVDF matrix. This in situ method was considered as a promising approach for better homogenous composites than traditional solution phase mechanical mixing and relevant methods [2, 25, 26]. Because of nucleation and growth in matrix, the fillers could be dispersed uniformly and enable good interactions between the fillers and the polymer matrix [27]. The size of the fillers also could be controlled by the flexible reaction time in the simple and low cost in situ process. In addition, enhanced electroactive β phase of PVDF, which plays a key role for improving the dielectric and piezoelectric performance of PVDF, were confirmed by the recent reports, such as metal Au and Ag [25], metal oxides ZnO [2], Fe_2O_3 [26], and salt $Ni(OH)_2$ [27].

A novel DIPAB/PVDF all-organic composite was discovered, and DIPAB nano-crystal was designed in situ growth in PVDF matrix. We found that the orientation structures of DIPAB and PVDF matrix interacted effectively by each other. The dielectric permittivity of the PVDF was markedly improved by an even lower concentration of the DIPAB loading. The composite films remain robust even in high breakdown electric fields. And the effect of structure transformation on the dielectric properties was analyzed in this paper.

2 Experimental

2.1 Raw materials

The PVDF polymer was purchased from 3F Co., China. The *N,N*-dimethylformamide (DMF) was purchased from Fuyu Co., China. The monomers and solvent were used as the raw materials without further purification. Diisopropylammonium bromide (DIPAB) was generated by equal

molar amounts of diisopropylamine and hydrobromic acid slow in the aqueous solution. The solution was heated and then salt precipitation of DIPAB separated them. Afterwards, DIPAB is heated to 426 K and maintained for half an hour using the oven.

2.2 Synthesis of DIPAB/PVDF composite films

The DIPAB/PVDF composite films were synthesized by in situ growth method. Initially, DIPAB of crystalline powder was added in the solvent of *N,N*-dimethylformamide (DMF) and then it dissolved using sonication. Next, the mixture was introduced in the polymer matrix of PVDF, which was continuously stirred for 2 h at room temperature. The mixed solution was kept in a vacuum oven at room temperature for 1 h before being cast onto a cleaned glass substrate with an automatic film applicator. The sticky film was kept in a vacuum oven at room temperature for 30 min to let the entrapped air out naturally. Subsequently, the final solution was poured onto a glass plate to form a cast film through a four-step cure processes (40 °C/1 h, 60 °C/1 h, 80 °C/1 h, 100 °C/20 h) under an air atmosphere in an oven. On cooling, the films were stripped off the glass surface and characterized. The average thickness of the film was 57–60 μm in final product. The detail DIPAB doping concentrations were given in Table 1. A schematic diagram of the fabrication of DIPAB/PVDF composite films was shown in Fig. 1.

2.3 Characterization

The samples were investigated using X-ray diffractometer (X'Pert PRO, PANalytical, Netherlands) with Cu Kα radiation (Kα = 0.1541 nm) and 2θ varying from 10 to 50 under a voltage of 40 kV. The samples were then characterized using a Fourier transform infrared spectroscopy (FTIR) (Avatar 370, Thermo Nicolet Corporation, and America) to determine the effect of DIPAB on β phase crystallization. The absorbance data of the films with thickness 15–17 μm were studied from 400 to 1000 cm^{-1}. The morphology and microstructures of pure PVDF and DIPAB doped PVDF films were investigated using a Polarizing microscope (BX51, OLYMPUS). The dielectric properties were investigated using a digital LCR meter (Agilent, 4294A). The capacitance (C) and loss tangent were recorded in the frequency range 40 Hz–15 MHz at room temperature across the two opposite surfaces with holder contained circular Aluminum electrodes of the samples. The relative dielectric constant (ε_r) of the samples was calculated using following Eq. (1),

$$\varepsilon_r = C \cdot d/(\varepsilon_0 \cdot S) \quad (1)$$

where d and S are the thickness and area of the samples, respectively. And ε_0 is vacuum permittivity with a value of 8.854×10^{-12} F/m. The admittance (Y) and angle (θ) were recorded in the frequency range 40 Hz–15 MHz using a digital LCR meter (Agilent, 4294A). The AC conductivity (σ_{AC}) of the samples was calculated using (2),

$$\sigma_{AC} = Y \cdot d \cdot \cos(\theta)/S \quad (2)$$

The electric breakdown strength was tested with an adielectric withstand voltage test (YD2013, Changzhou Yangzi Electronic Co., Ltd) with ten simple tests to increase the accuracy in 50 Hz.

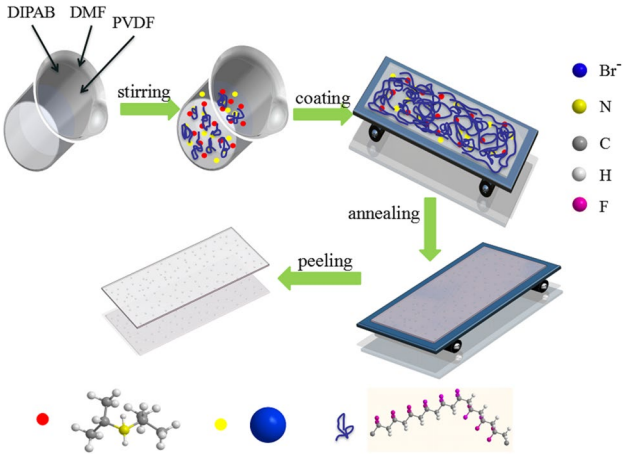

Fig. 1 schematic diagrams of the fabrication of DIPAB/PVDF composite films

Table 1 Detail of the sample identification

Sample name	Amount of PVDF (g)	Percentage of salts (mass%)	Amount of salts (g)
PVDF	4.7250	0	0
DIPAB1	4.7250	1	0.0486
DIPAB5	4.7250	5	0.2487
DIPAB10	4.7250	10	0.5248
DIPAB15	4.7250	15	0.8338
DIPAB20	4.7250	20	1.1816

3 Results and discussions

3.1 Structure of DIPAB/PVDF composite films

The crystallization behavior of pure PVDF and DIPAB doped PVDF composite films have been studied by X-ray diffractometer, as shown in Fig. 2. The XRD spectrum of pure PVDF shows diffraction peaks at 18.3° corresponded to non-polar α phase and a tiny peak at 38.3° assigned to

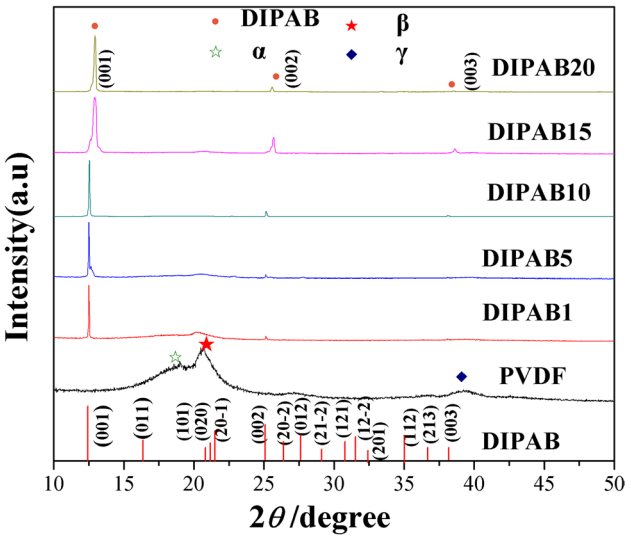

Fig. 2 XRD patterns of DIPAB/ PVDF composite films

the polar γ phase [28]. The peaks at 2θ corresponded to 20.3° and confirmed the presence of the β phase PVDF [29]. And the crystallographic indexing was delivered according to the diffraction pattern of DIPAB [24, 30]. It is very interesting that the in situ grown DIPAB crystal possess perfect (00*l*) orientation. The diffraction peaks around 12.4°, 25.1° and 38.4° were confirmed to (001), (002) and (003) reflections of DIPAB crystal [30]. The preferential (00*l*) orientation indicates the strong interaction between the PVDF matrix and DIPAB crystal particles. The interaction taken place on the surfaces of the growing particles, and whose structure influenced by the $–CH_2$ and $–CF_2$ dipolar groups in PVDF.

3.2 Nucleation of electroactive β phase of PVDF composite films

The nucleation of electroactive β phase was investigated by FTIR spectra in the films. Figure 3a displays the FTIR spectra of pure PVDF and DIPAB-doped PVDF thin films. The absorbance spectrum of pure PVDF represents bands around 480 cm^{-1} (CF_2 waging), 529 cm^{-1} (CF_2 bending), 609, 760 cm^{-1} (CF_2 bending and skeletal bending), 798 and 973 cm^{-1} (CH_2 rocking) ascribed to α-phase and the small band at 840 cm^{-1} (CH_2 rocking, CF_2 stretching and skeletal C–C stretching) which is due to β phase [29, 30]. The absorbance bands of the non-polar α phase vanished and the bands assigned to electroactive β phase began to emerge prominently including 445 cm^{-1} (CF_2 rocking and CH_2 rocking), 475 cm^{-1} (CF_2 deformation) 510 cm^{-1} (CF_2 stretching), 598 cm^{-1} (CF_2 waging), and 840 cm^{-1} (CH_2 rocking, CF_2 stretching and skeletal C–C stretching) after the DIPAB particles grown in PVDF [29, 31].

The relative fraction of β phase content (F[β]) in the DIPAB-loaded PVDF composite films was evaluated. The variation of F(β) (%) has been shown with DIPAB content (mass%) in Fig. 3b. The results show that the DIPAB crystal particles could increase the content of the β phase nucleation in PVDF matrix and attained a maximum value of 78.79% at 5 mass% doping of DIPAB crystal particles. Therefore, it is quite sure that due to the large electronegativity of the fluorine atoms in PVDF and the surface charge of in situ growth DIPAB particles an interaction takes place in order to minimize the potential for a stereo-chemical conformation that eventually induces the β phase [25]. It is considered that this interaction not only enhances the β phase transformation from α phase but also improves the (00*l*) orientation of the in situ growth DIPAB particles,

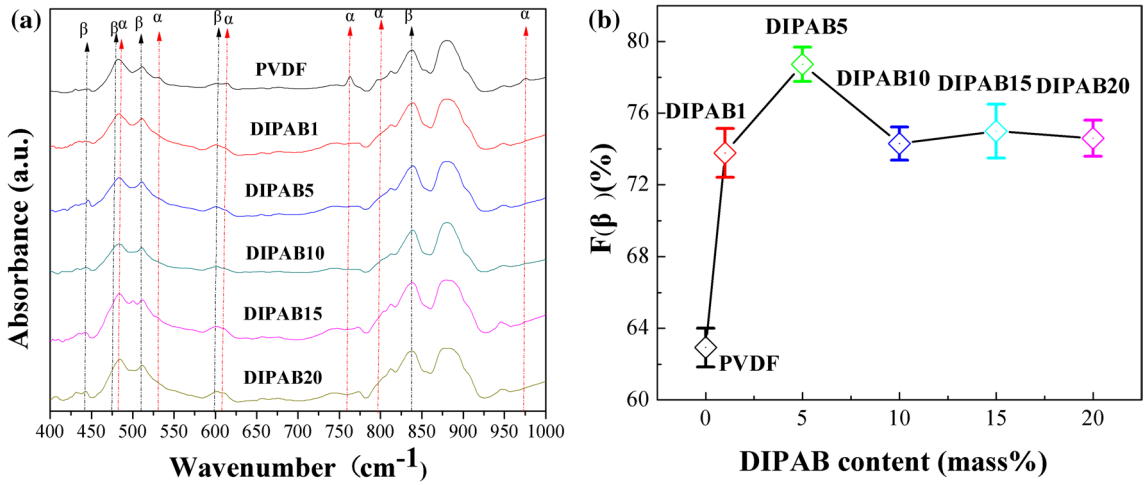

Fig. 3 **a** FTIR spectra of pure PVDF and DIPAB doped PVDF thin films and **b** evaluation of β-phase content with increasing DIPAB content form IR spectra

which would strengthen the dielectric performance of the composites.

3.3 Morphology of DIPAB/PVDF composite films

The morphology and microstructures of pure PVDF and DIPAB-doped PVDF films were investigated using a polarizing microscope. Figure 4 shows the polarizing microscope images of (a) pure PVDF and surface of (b) DIPAB1, (c) DIPAB5, (d) DIPAB10 and (e) DIPAB15. The in situ growth DIPAB crystal particles were uniformly dispersed and fully encapsulated in PVDF matrix including with 5 mass% concentrations, as shown in Fig. 4c. With increasing DIPAB crystal content, the DIPAB crystals gradually covered the surface of DIPAB/PVDF composite films and formed a crystal films as can be seen in Fig. 4d DIPAB10 and (e) DIPAB15. It is important to point out that the composite films possess good flexible performance even with high doping concentration as shown in Fig. 4f.

3.4 Dielectric properties

3.4.1 Frequency dependence of the dielectric properties

Figure 5a shows the frequency dependence of the relative dielectric constant of pure PVDF and the DIPAB-loaded PVDF composite films at room temperature. The data show that the relative dielectric of all the composite films

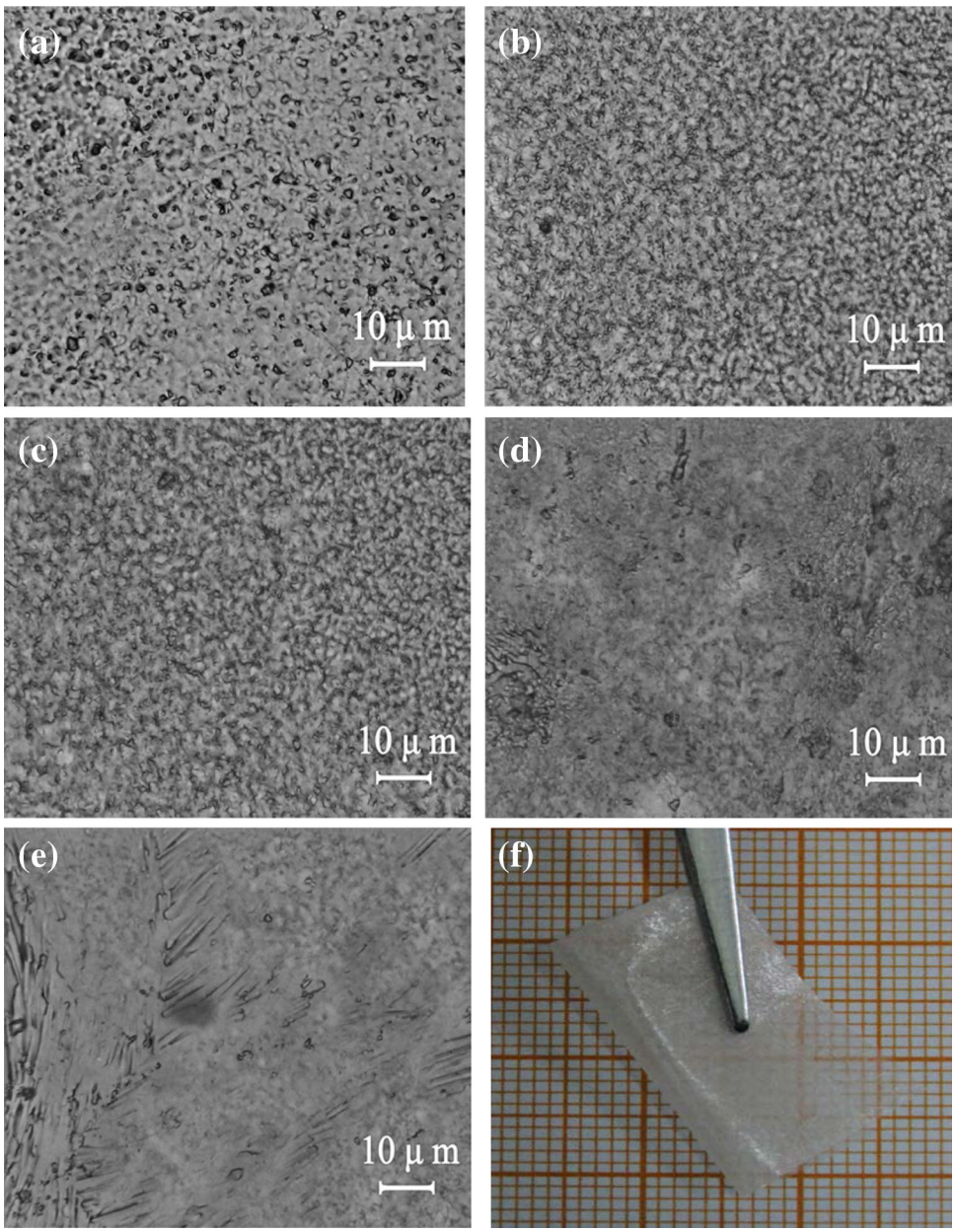

Fig. 4 Polarizing microscope images of **a** pure PVDF and surface of **b** DIPAB1, c DIPAB5, **d** DIPAB10, **e** DIPAB15 and **f** DIPAB20

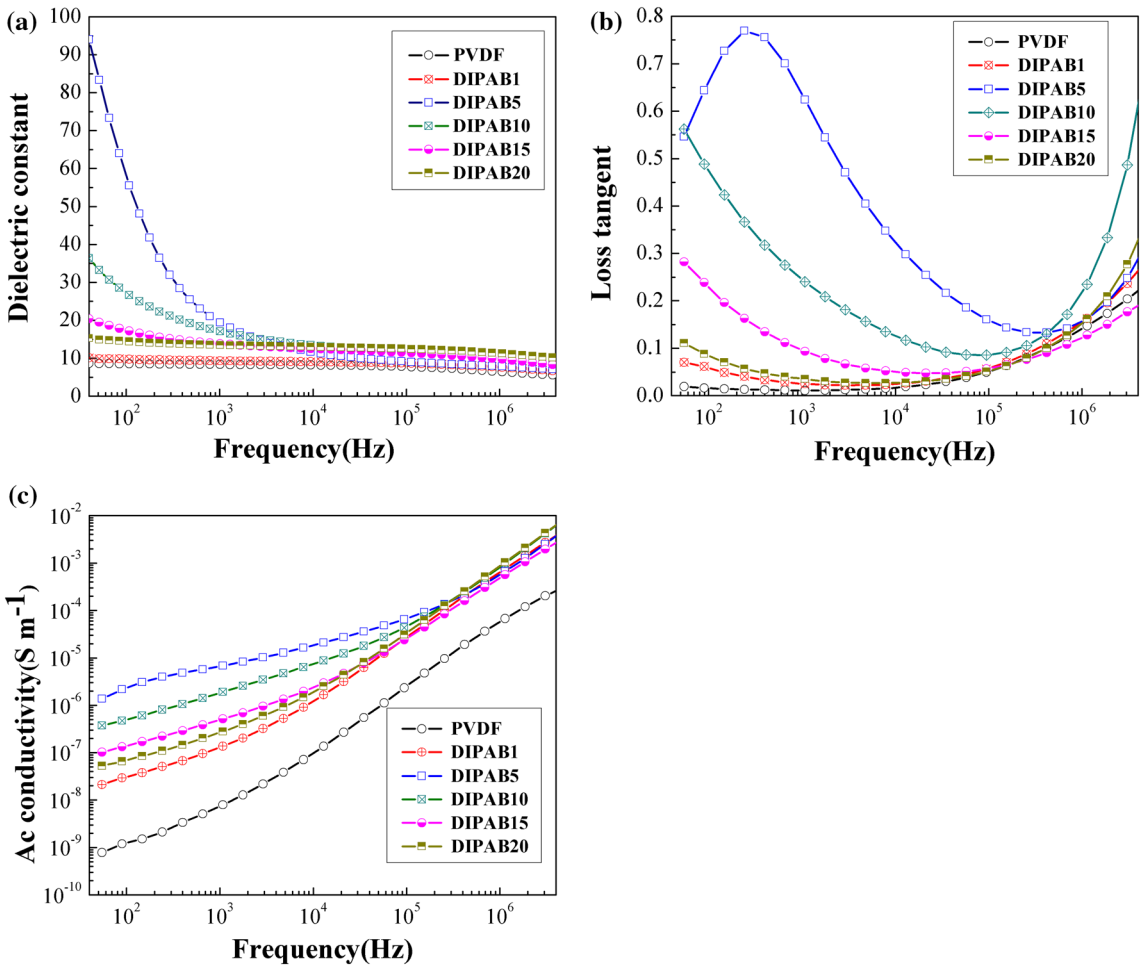

Fig. 5 Frequency dependence of dielectric properties of DIPAB/PVDF composite films: **a** Dielectric constants, **b** loss tangent and **c** ac conductivity

decreases with increasing frequency because of the reduction in the effective number of dipoles. The dipoles could keep up with changing frequency at low frequency. However, the dipoles begin to lag frequency with increasing frequency rotation in the AC electric field, which reduces the number of effective dipoles [32–34].

The interfacial polarization mechanism was used to explain the relative dielectric constant of the PVDF composite films that decreases with increasing frequency. When the electric field is applied to the sample, the charge carriers from the electrode and/or the impurities of the composites can migrate and accumulate at the interface between the filler and polymer due to the large difference in electrical conductivity between the polymer matrix and the filler [35]. The charge carrier migrated, and the cumulative process can cause large polarization and a relative constant dielectric. At this low frequency, this movement and accumulation process continues smoothly due to a charge carrier or dipole getting enough time for their movement. Accordingly, the migrated and cumulative charge carrier at the interface led to large polarization and dielectric constant [34]. With increasing frequency, the charge carriers or dipole movement is limited due to the frequency mismatch [36]. Consequently, the relative dielectric constant decreases—this was observed with increasing frequency for all samples. The relative dielectric constant was 94 for the film with DIPAB5 at 40 Hz.

Figure 5b shows that the loss tangent decreases and then increases with increasing frequency. The loss tangent decreased with increasing frequency due to the Maxwell–Wagner–Sillars (MWS) effect [37]. The DIPAB5 film shows a tangent loss peak at 200–300 Hz that might because it reached the characteristic value of frequency (1/t) [31]. The loss tangent increased with increasing frequency due to a loss in conductance. Figure 5c shows that the AC conductivity increased with increasing frequencies for all DIPAB samples. The highest ac conductivity is in DIPAB5 at about 1.25×10^{-6} S/m at 40 Hz.

3.4.2 *Dependence of dielectric properties on DIPAB content*

Figure 6a, b shows the variation of the relative dielectric constant and loss tangent of pure PVDF and DIPAB doped PVDF composite films at 100 Hz. The relative dielectric constant increases sharply for DIPAB-loaded polymer films up to 5.0 mass% doping of DIPAB. It decreases at higher doping contents—this may because a critical point is reached (Fig. 6a). When the DIPAB-doped crystal particles reached 5 mass%, the DIPAB crystal particles were uniformly dispersed and formed sufficiently small particles in the polymer. The contact area increases between the crystalline particles of DIPAB and PVDF matrix. This results in a great interfacial polarization. Thus, this will greatly increase the dielectric constant of the composite films. The maximal dielectric permittivity is 61 and found for the DIPAB samples.

The enhancing dielectric properties explain two main aspects. On the one hand, interfacial polarization effects emerges in a heterogeneous medium consisting of phases with different relative dielectric constants and ac conductivity values due to the accumulation of charges at the interfaces. The crystal particles of DIPAB are well separated from each other with no such effective interaction between them at low DIPAB concentrations. As DIPAB content increases, the crystal particles of DIPAB and their interfacial area per unit mass increases while the inter-particle distance decreases [26]. This improves the average polarization associated with the coupling between neighboring grains and leads to a giant dielectric enhancement of the composite films. The dielectric properties of the samples can be observed from their microstructure to explain these findings. The good homogeneous dispersion of the DIPAB in the PVDF matrix is up to 5.0 mass% loading of DIPAB. This leads to more interfacial area per unit mass of the DIPAB, which improves the interfacial polarization for the samples. Higher doping concentrations of the DIPAB could decrease the interfacial area per unit mass due to agglomeration of the crystal DIPAB. This decreases the dielectric

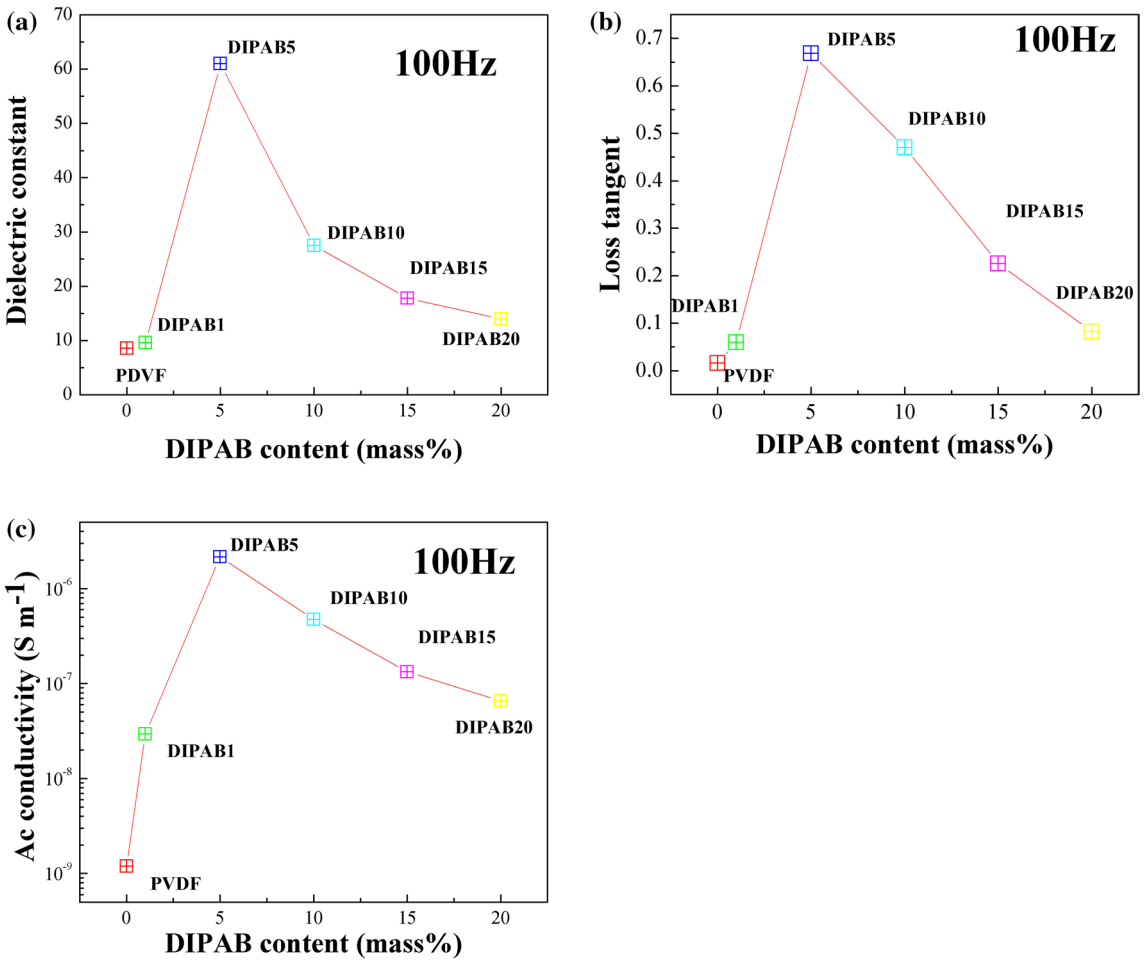

Fig. 6 DIPAB content dependence of dielectric properties of DIPAB/PVDF composite films; **a** dielectric permittivity, **b** loss tangent and **c** ac conductivity

constant and ac conductivity [26, 34]. On the other hand, the enhancing dielectric properties were attributed to the increased electroactive β phase content in the polymer samples and the preferential (00*l*) orientation of the in situ growth DIPAB crystal. It can be seen clearly from the XRD and FTIR spectra that an interaction takes place in the interface between the in situ growth DIPAB crystal and PVDF matrix. The phase transformation from α phase to β phase was enhanced by the influence of in situ growth DIPAB particles because of the strong spontaneous polarization of DIPAB crystal; whereas, the preferential (00*l*) orientation of DIPAB crystal was significantly affected by the large electronegativity of the fluorine atoms in PVDF during the in situ growth process. Therefore, this interaction would be beneficial to the dielectric performance of the DIPAB-loaded samples.

3.5 Dielectric breakdown strength and energy density of DIPAB/PVDF composite films

The dielectric breakdown fields of the DIPAB/PVDF composite films were measured in the surrounding environment. The Weibull distribution [38] was introduced to analyze the dielectric breakdown strength. Figure 7 shows that the breakdown strength declined with increasing DIPAB content. This might be attributed to the increasing inner space charges generated from the introduction of organic particles [16]. The space charges accumulate, and the inner electric field becomes unbalanced leading to a breakdown in materials. In addition, the electric field near the interface between the DIPAB crystal particles and the matrix was enhanced due to the differences in the electric properties between the fillers and the polymer matrix. The breakdown strength decreased slowly when the addition exceed 5 mass%. Despite this large decrease in breakdown strength that occurred in the low loading of DIPAB powder, the DIPAB/PVDF composite films with the DIPAB content over 15 mass% still withstood a high breakdown strength. When 20 mass% DIPAB crystal particles were added, the breakdown strength was 38.9 kV/mm.

The energy density is related to the relative dielectric constant and the breakdown strength, according to the energy density formula as follows [16],

$$U = 1/2\varepsilon_o\varepsilon_r E^2 \tag{3}$$

where ε_o, ε_r and E are the vacuum dielectric constant, the relative dielectric constant and the breakdown strength, respectively. As shown in Fig. 8, the energy density increases as the increasing mass fraction of DIPAB. The energy density was about 1.38 J/cm^3 with 5 mass%, and then it decreases when the doping concentration exceed 5 mass%. It also can be seen from Fig. 6 (a) that the relative permittivity of the composite increases first with the increase of DIPAB doping content, and decreases when the doping concentration reaches 5 mass%. It can also be observed in Fig. 8 that the breakdown strength decreases as the doping concentration of DIPAB increases. Therefore, both the relative dielectric constant and the breakdown strength are the direct issues for the variation of the energy density with DIPAB doped PVDF films.

4 Conclusion

The novel all organic DIAPB/PVDF composite flexible film with significant dielectric properties has been successfully fabricated through an in situ growth method. Electroactive β phase and (00*l*) textured DIPAB were observed in the composites. And an obvious increase of Electroactive

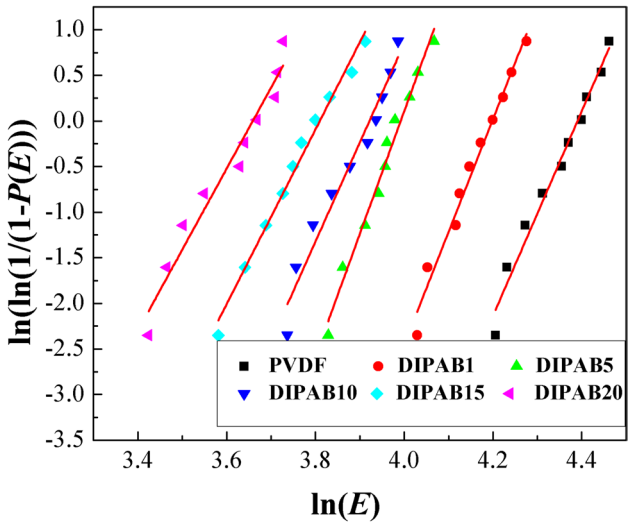

Fig. 7 Weibull distribution of DIPAB/PVDF composite films

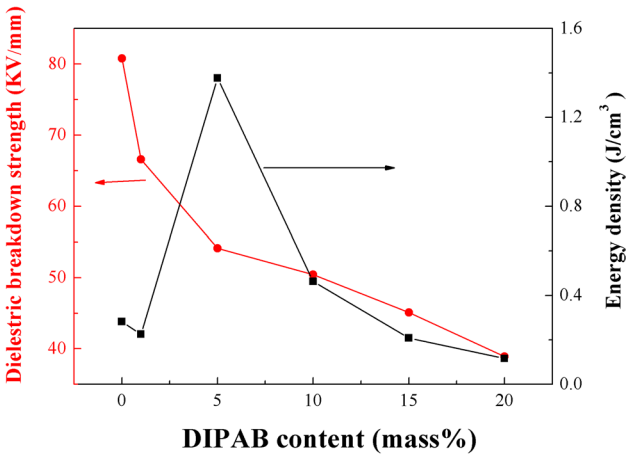

Fig. 8 Dielectric breakdown strength and energy density of DIPAB/PVDF composite films

β phase was also found by the increasing content of in situ growth DIPAB particles. Fourier transform infrared spectroscopy results showed the optimal content 78.79% of β phase in PVDF matrix with 5 mass% doping of DIPAB crystal particles. Strong interaction was confirmed on the interface between the particles and the PVDF matrix due to the large electronegativity of the fluorine atoms in PVDF and the surface charge of in situ growth DIPAB particles. It is considered that this interaction not only enhances the β phase transformation from α phase but also improves the (00*l*) orientation of the in situ growth DIPAB particles, which would strengthen the dielectric performance of the composites. Relative dielectric constant as high as 94 was obtained at 40 Hz, which is 11-fold higher than that of the pure, PVDF matrix when the concentration of the DIPAB filler reached 5 mass%, (~8.5). Weibull distribution was adopted to analyze the dielectric breakdown strength, which showed that the breakdown strength of DIPAB/PVDF composite film with 5 mass% doping of DIPAB crystal particles was 54.11 KV/mm and the E_b decreased as the mass fraction of DIPAB increased but still stronger than 38.9 kV/mm.

Acknowledgements Authors are highly thankful to the National Natural Science Foundation of China (Grant Nos. 11444004 and 61372013), the National Natural Science Foundation of Heilongjiang Province (Grant No. E201258), the Program of Harbin Innovative Scientist (Grant No. 2013RFXXJ068) for project.

References

1. D. Bhadra, SC. Sarkar, BK. Chaudhuri, RSC Adv. **5**, 36924–36932 (2015)
2. Z. Li, X. Zhang, G. Li, Phys. Chem. Chem. Phys. **16**, 5475–5479 (2014)
3. M. Feng, X. Huang, Z. Pu, X. Liu, J. Mater. Sci. **25**, 1393–1399 (2014)
4. S. Liu, S. Xue, W. Zhang, J. Zhai, G. Chen, J. Mater. Chem. A **42**, 18040–18046 (2014)
5. P. Khanchaitit, K. Han, M.R. Gadinski, Q. Li, Q. Wang, Nat. Commun. **4**, 1–7 (2013)
6. Y. Song, Y. Shen, H. Liu, Y. Lin, M. Li, C.W. Nan, J. Mater. Chem. **32**, 16491–16498 (2012)
7. B.J. Madhu, M. Gurusiddesh, T. Kiran, B. Shruthi, H.S. Jayanna, J. Mater. Sci. **27**, 7760–7766 (2016)
8. Z.M. Dang, J.K. Yuan, S.H. Yao, R.J. Liao, Adv. Mater. **44**, 6334–6365 (2013)
9. W. Wu, X. Huang, S. Li, P. Jiang, T. Toshikatsu, J. Phys. Chem. C **47**, 24887–24895 (2012)
10. X. Zhang, Y. Ma, C. Zhao, W. Yang, Appl. Surf. Sci. **305**, 531–538 (2014)
11. W. Zhu, W. Ren, H. Xin, P. Shi, X. Wu, J. Adv. Dielectr. **2**, 1350011 (2013)
12. P. Bharathi, K.B.R. Varma, J. Appl. Phys. **16**, 164107 (2014)
13. J. Lin, G. Chen, W. Yang, Z. Jiang, H. Li, L. Wang, Q. Lei, Appl. Phys. A **122**, 1–9 (2016)
14. S. Cho, J.S. Lee, J. Jang, ACS Appl. Mater. Interfaces **18**, 9668–9681 (2015)
15. Z. Ahmad, A. Prasad, K. Prasad, Phys. B **404**, 3637–3644 (2009)
16. B. Luo, X. Wang, Y. Wang, L. Li, J. Mater. Chem. A **2**, 510–519 (2014)
17. T. Chen, Y. Zhao, L. Pan, M. Lin, J. Mater. Sci. **26**, 10164–10171 (2015)
18. Z.M. Dang, B. Peng, D. Xie, S.H. Yao, M.J. Jiang, J. Bai, Appl. Phys. Lett. **11**, 112910 (2008)
19. Z.M. Dang, Y.H. Lin, C.W. Nan, Adv. Mater. **15**, 1625–1629 (2003)
20. L. Wang, Z.M. Dang, Appl. Phys. Lett. **4**, 042903 (2005)
21. Q.M. Zhang, H. Li, M. Poh, F. Xia, Z.Y. Cheng, H. Xu, C. Huang, Nature **419**, 284–287 (2002)
22. J. Wang, Y.E. Wang, S. Li, J. Xiao, J. Polym. Sci. **4**, 490–495 (2010)
23. K. Shehzad, A. Ul-Haq, S. Ahmad, M. Mumtaz, T. Hussain, A. Mujahid, F. Nawaz, J. Mater. Sci. **10**, 3737–3744 (2013)
24. D.W. Fu, H.L. Cai, Y. Liu, Q. Ye, W. Zhang, Y. Zhang, R.G. Xiong, Science **6118**, 425–428 (2013)
25. D. Mandal, K. Henkel, D. Schmeißer, Mater. Lett. **73**, 123–125 (2012)
26. P. Thakur, A. Kool, B. Bagchi, S. Das, P. Nandy, Phys. Chem. Chem. Phys. **17**, 1368–1378 (2015)
27. P. Thakur, A. Kool, B. Bagchi, N.A. Hoque, S. Das, P. Nandy, Phys. Chem. Chem. Phys. **17**, 13082–13091 (2015)
28. G. Chen, X. Wang, J. Lin, W. Yang, H. Li, Y. Wen, J. Mater. Chem. C **4**, 8070–8076 (2016)
29. C. Thirmal, P.P. Biswas, Y.J. Shin, T.W. Noh, N.V. Giridharan, A. Venimadhav, P. Murugavel, J. Appl. Phys. **120**, 124107 (2016)
30. P. Thakur, A. Kool, B. Bagchi, S. Das, P. Nandy, Appl. Clay Sci. **99**, 149–159 (2014)
31. P. Thakur, A. Kool, B. Bagchi, N.A. Hoque, S. Das, P. Nandy, RSC Adv. **5**, 62819–62827 (2015)
32. L. Flandin, L. Vouyovitch, A. Beroual, J.L. Bessède, N.D. Alberola, J. Phys. D **38**, 144 (2004)
33. J. Pu, Y. Yomogida, K.K. Liu, L.J. Li, Y. Iwasa, T. Takenobu, Nano Lett. **8**, 4013–4017 (2012)
34. C. Lopes, C.M. Costa, R.S. i Serra, I.C. Neves, J.G. Ribelles, S. Lanceros-Méndez, Solid State Ion. **235**, 42–50 (2013)
35. P. Lunkenheimer, V. Bobnar, A.V. Pronin, A.I. Ritus, A.A. Volkov, A. Loidl, Phys. Rev. B **5**, 052105 (2002)
36. R.G. Lorenzini, W.M. Kline, C.C. Wang, R. Ramprasad, G.A. Sotzing, Polymer **54**, 3529–3533 (2014)
37. Y. Li, X. Huang, Z. Hu, P. Jiang, S. Lia, T. Tanaka, ACS Appl. Mater. Interfaces **11**, 4396–4403 (2011)
38. W. Weibull, J. Appl. Mech. **18**, 293–297 (1951)